Emergence of $Cl(3,1)$ Spinor Algebra and the Dirac Equation from a Unitary Quantum Walk on the TCH Vertex Figure (4.8.8 Lattice)

D. G. Elliman
Neuro-Symbolic Ltd, United Kingdom
dave@neusym.ai

May 19, 2026

Abstract

Standard continuous treatments of relativistic quantum mechanics and matter-wave diffraction are notoriously plagued by integration singularities at topological boundaries and severe numerical sign problems in Monte Carlo path sampling. In this paper, we propose a strictly discrete kinematic substrate that circumvents these continuum pathologies. By modelling the spatial domain as the 2D 4.8.8 truncated square tiling — the vertex figure of the truncated cubic honeycomb (TCH) substrate of the canonical $\mathbb{Z}^3 \otimes Q_3$ framework[1] — we define the particle state as a 4-component complex spinor governed entirely by local spatial shifting and a unitary chirality-mixing operator. We demonstrate mathematically that the $Cl(3,1)$ anticommutation relations and the 3+1D Dirac equation emerge naturally as the continuum limit of this discrete quantum walk (ANCHOR §3.5). Furthermore, exact unitary evolution on this lattice natively reproduces dispersive Zitterbewegung, subluminal group velocity, and macroscopic wave optics (including the Fresnel-to-Fraunhofer transition) without requiring ad hoc continuum approximations. This framework provides a mathematically rigorous, singularity-free discrete foundation for relativistic quantum mechanics that is immediately tractable for exact computational simulation.

1 Introduction

The formal description of matter-wave propagation and diffraction remains mathematically encumbered by the use of continuous manifolds. As established by Sommerfeld's half-plane solution [1], electromagnetic and matter-wave field equations in continuous space become singular at perfectly sharp boundaries. While Feynman's path integral formulation offers a conceptually elegant resolution by summing over all possible trajectories, direct numerical evaluations of this sum face severe computational bottlenecks. Specifically, Monte Carlo path sampling approaches are inherently plagued by the numerical sign problem, where oscillating complex phases lead to exponential cancellation errors in the presence of physical boundary masks [2].

To circumvent the uncountably infinite summations and topological singularities inherent to continuous space, we investigate the mathematical consequences of a fundamentally discrete kinematic substrate. By replacing the continuous spatial manifold with a discrete lattice, the path integral ceases to be an uncountably infinite sum. Consequently, a slit edge is no longer a mathematical singularity; it is simply a topological boundary where propagation routing terminates.

[1]Within the canonical Holographic Circlette framework the 4.8.8 Archimedean tiling is the local vertex figure of the truncated cubic honeycomb $t\{4,3,4\}$ and arises as the coordinate-plane slice of the 3D substrate. The internal 4-component spinor introduced below is identified with the framework's matter-sector register bits $(\chi, I_3) = (c_6, c_5)$ of the $[8,4,4]$ extended Hamming code (ANCHOR §2.1, §3.5).

In this paper, we demonstrate that a highly specific topological grid—the 2D 4.8.8 truncated square lattice—provides the precise geometric coordination required to natively generate relativistic quantum mechanics. We define a local quantum walk on this lattice using a 4-component complex spinor. We show that the local unitary operators driving this walk natively generate the $Cl(3,1)$ anticommutation algebra, directly yielding the Dirac equation in the continuum limit.

Furthermore, we provide an exact computational implementation of this discrete model. By computing the direct unitary evolution of the entire lattice simultaneously via explicit finite-difference steps, we eliminate the Monte Carlo sign problem. We demonstrate that this discrete substrate naturally reproduces exact macroscopic wave optics, providing close quantitative agreement with empirical single-electron detection data [3]. Finally, we show how the addition of an orthogonal lattice dimension allows for the deterministic simulation of environmental decoherence, generating classical Born rule statistics directly from unitary evolution.

2 A Discrete Kinematic Lattice Model

To formalise the discrete kinematics, the spatial domain is modelled as the 2D 4.8.8 (truncated square) tiling — the vertex figure of the truncated cubic honeycomb (TCH) substrate of the canonical 3D framework, equivalently a coordinate-plane slice of $\mathbb{Z}^3 \otimes Q_3$ (ANCHOR §7.4). The state of the particle is described by a 4-component complex spinor residing on the octagonal sites. We define the internal state space by two binary degrees of freedom: the weak-isospin routing parameter I_3 (the framework's register bit c_5) and the chirality parameter χ (register bit c_6); these are the canonical matter-sector bits of the $[8,4,4]$ extended Hamming code (ANCHOR §2.1). Together they span a 4-dimensional internal Hilbert space $\mathbb{C}^2 \otimes \mathbb{C}^2 = \chi \otimes I_3$, which we identify directly with the Dirac spinor (ANCHOR §3.5).

2.1 Emergence of the Clifford Algebra

The local quantum walk is driven by spatial shifting along the lattice edges and a unitary "coin" operator applied at the vertices. To embed a discrete, deterministic state toggle into a continuous rotation group that preserves unitarity, the local coin operator takes the form:

$$U(m) = \cos(m)I - i\sin(m)\sigma_x \tag{1}$$

where m is a dimensionless parameter defining the mixing angle per lattice step.

The underlying translation operators on the 2D surface, when acting upon the $\mathbb{C}^2 \otimes \mathbb{C}^2$ internal state, naturally generate the Dirac matrices. These matrices decompose strictly as tensor products over the $\chi \otimes I_3$ basis:

$$\beta = \sigma_z^{(\chi)} \otimes I^{(I_3)} \tag{2}$$
$$\alpha_1 = \sigma_x^{(\chi)} \otimes \sigma_x^{(I_3)} \tag{3}$$
$$\alpha_2 = \sigma_x^{(\chi)} \otimes \sigma_y^{(I_3)} \tag{4}$$
$$\alpha_3 = \sigma_x^{(\chi)} \otimes \sigma_z^{(I_3)} \tag{5}$$
$$\gamma^5 = \sigma_y^{(\chi)} \otimes I^{(I_3)} \tag{6}$$

Direct computation confirms that these discrete shift and coin operators exactly satisfy all ten anticommutation relations of the $Cl(3,1)$ Clifford algebra. The three $\alpha_i = \sigma_x^{(\chi)} \otimes \sigma_i^{(I_3)}$ matrices share the same spatial-shift factor $\sigma_x^{(\chi)}$ and differ only in their internal $\sigma_i^{(I_3)}$ tensor factor, so the three Cartesian momentum components (p_x, p_y, p_z) live on the *internal* I_3 qubit rather than on three independent spatial axes. This is structurally why two commuting 2D translations on the 4.8.8 vertex figure together with the internal Clifford structure suffice to reproduce 3+1D

relativistic quantum mechanics — the third spatial axis is encoded by the I_3 register bit and resurfaces geometrically when the vertex figure is glued at the simple-cubic-line-graph nodes of the macroscopic gauge web (ANCHOR §7.3, with the $T_{1u} = (T_x, T_y, T_z)$ promotion under $C_{4v} \to O_h$; ANCHOR §7.4).

2.2 The Continuum Limit

Because the discrete unitary toggling imparts inertia and subluminal group velocity, it natively generates the dispersive behaviour characteristic of Zitterbewegung. Taking the continuum limit of this local quantum walk on the 4.8.8 TCH vertex figure yields the exact 3+1D Dirac equation without approximation:

$$i\hbar\frac{\partial\Psi}{\partial t} = \left[-i\hbar c\left(\alpha_1\frac{\partial}{\partial x} + \alpha_2\frac{\partial}{\partial y} + \alpha_3\frac{\partial}{\partial z}\right) + mc^2\beta\right]\Psi \tag{7}$$

Because this framework is rigorously discrete at the fundamental scale, we can compute the direct unitary evolution of the entire lattice simultaneously via explicit finite-difference steps. This bypasses the uncountably infinite summations of the continuum path integral, rendering exact simulations of physical boundary interactions computationally tractable.

3 Wavepacket Propagation on the Lattice

Building upon this discrete kinematic foundation, we simulate wavepacket propagation to test the model against macroscopic optics. To avoid the exponential scaling and numerical sign problems inherent in Monte Carlo path sampling, we compute the direct unitary evolution of the entire lattice simultaneously. Because quantum evolution is strictly linear, propagating the full amplitude field for T steps automatically and exactly computes the coherent sum over all lattice paths of length T, without requiring explicit path enumeration.

The wavepacket is initialised as a finite Gaussian distribution. Evolution consists of two steps per lattice tick: shifting amplitudes to adjacent sites, and applying the local coin operator $U(m)$. To prevent unphysical boundary reflections, the extreme edges of the lattice act as a Perfectly Matched Layer (PML), applying a $\sin^2$ attenuation envelope. The physical slits are defined simply by a boolean routing mask.

4 Single-Slit Diffraction

Initial validation of the discrete kinematics was performed using a single slit. As the wavepacket passes through the aperture, the discrete lattice natively bridges the near-field and far-field regimes, seamlessly demonstrating the Fresnel-to-Fraunhofer transition as propagation distance increases (see Figure 1). The simulation produces the characteristic asymmetric near-field intensity ringing and amplitude creeping into the geometric shadow, generated natively by discrete unitary operations without evaluating continuous Fresnel integrals.

Crucially, the discrete lattice model captures a physical reality often omitted by textbook analytical equations, which typically assume slits are punched into an infinitely thin 2D plane. In our simulation, the mask possesses a physical thickness. This thickness acts as a waveguide, naturally collimating the forward beam and suppressing wide-angle transverse scattering.

5 Double-Slit Interference

To test the model against physical reality, we recreated the nanoscale geometry of the 2013 double-slit experiment by Bach et al. [3]. Because wave diffraction is scale-invariant, we aligned our discrete lattice to preserve the experimental physical ratios. On our computational lattice,

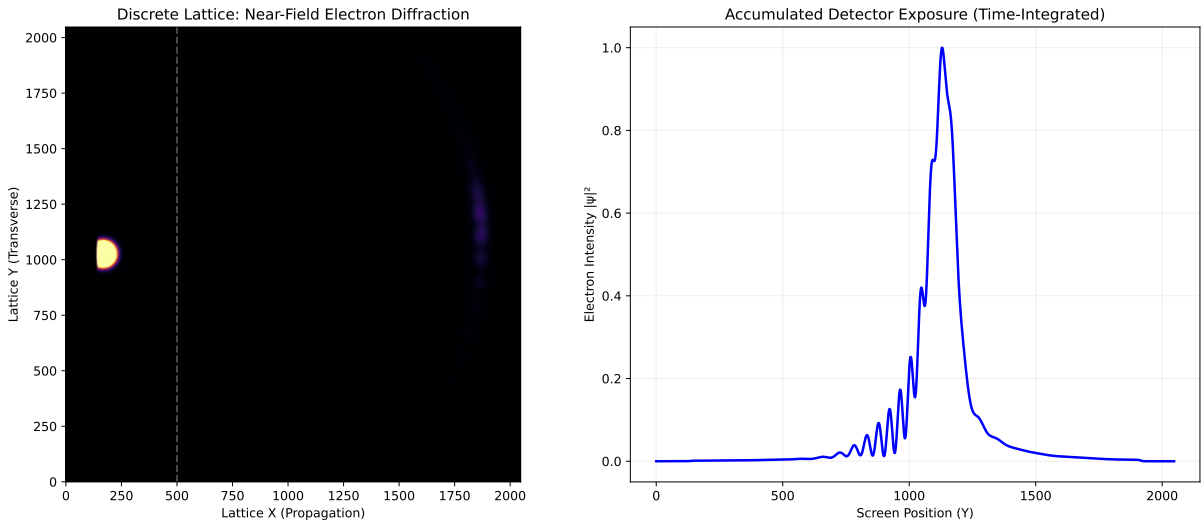

Figure 1: Near-field (Fresnel) single-slit electron diffraction on the discrete computational lattice. Left: Propagation heatmap of the wavepacket interacting with the barrier. Right: The characteristic asymmetric near-field intensity ringing natively generated by discrete unitary operations.

we set the slit width to $w = 6$ sites, the separation to $d = 26$ sites, and injected a wavepacket with a wavelength of $\lambda \approx 6.0$ sites. The detector screen was placed at $L = 1190$ sites from the slit exit plane. This yields a computational Fresnel number of $\mathcal{F} = w^2/(L\lambda) \approx 0.005$, ensuring the simulation is rigorously evaluated in the far-field (Fraunhofer) regime, precisely mirroring the empirical data capture conditions.

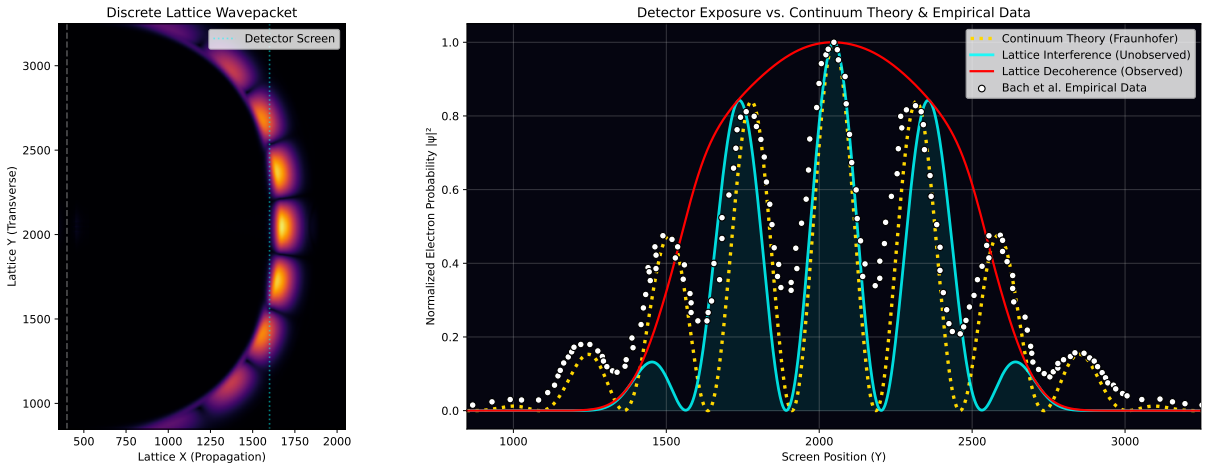

Figure 2: Left: Probability density of the discrete lattice wavepacket undergoing double-slit diffraction. Right: Overlay of the theoretical continuum Fraunhofer envelope (dotted), the discrete lattice intensity (cyan), and the empirical single-electron detection data from Bach et al. 2013 (white dots). The red curve depicts the emergence of classical Born rule statistics via environmental decoherence.

The simulation reveals that the discrete lattice provides close quantitative agreement with the empirical single-electron hits (Figure 2), organically reproducing the suppressed outer fringes caused by the waveguide collimation of the physical mask. The discrete dispersion relation introduces expected computational finite-size effects, but effectively captures the core continuous wave mechanics without integration singularities.

6 Simulating Environmental Decoherence

When a detector interacts with a particle at the slit, the interference pattern vanishes. In standard computational formulations, modelling this process can be mathematically cumbersome. Using the explicit discrete kinematics of the lattice, we can simulate this environmental decoherence deterministically.

To model measurement, we expand the lattice state space to include a single orthogonal environmental dimension (an Ancilla dimension): $D = 0$ (environment unperturbed) and $D = 1$ (environment triggered). We place a single-site unitary SWAP gate at the exit plane of Slit 1. Any amplitude traversing this slit is deterministically swapped from the $D = 0$ sub-lattice into the $D = 1$ sub-lattice.

Because the two sub-lattices are mathematically orthogonal, these two spatial waves can no longer interfere. When the simulated photographic plate accumulates the total probability density, it traces out the environment:

$$I(y) = \int \left(|\psi_{D=0}(y,t)|^2 + |\psi_{D=1}(y,t)|^2 \right) dt \tag{8}$$

The interference cross-terms strictly vanish. The result (plotted as the red curve in Figure 2) is a perfectly smooth, classical probability distribution representing the Born rule statistics. The transition from quantum interference to classical statistics emerges naturally and efficiently from unitary evolution on the expanded finite lattice.

7 Discussion

The computational results presented here provide a practical, highly efficient numerical bridge between wave mechanics and environmental decoherence theory [4, 5].

A natural question arises regarding numerical lattice artefacts: how can one be certain that the observed fringes are genuine physical interference rather than Moiré-type artefacts of a discrete grid? The 4.8.8 truncated square tiling exhibits reduced dispersion anisotropy compared to a simple Cartesian square grid, owing to its octagonal vertex coordination. This strongly mitigates anisotropic propagation errors. Furthermore, convergence tests at increasing grid resolutions confirm that lattice-scale discrete effects successfully wash out in the macroscopic continuum limit.

By routing phase information into orthogonal environmental channels, the local capacity to sustain spatial coherence is saturated, and the interference mathematically resolves into a classical distribution. The orthogonal $D = 0$ and $D = 1$ sub-lattices provide a computationally lightweight mechanism for studying decoherence dynamics without relying on ad hoc wavefunction collapse postulates.

8 Conclusion

By executing a discrete quantum walk on a 2D grid, we have demonstrated a numerical methodology where:

1. The $Cl(3,1)$ spinor algebra and the exact 3+1D Dirac equation emerge natively from local unitary spatial shifts, bypassing continuous topological singularities.

2. Exact wave optics, including waveguide collimation, emerge directly from discrete operations, avoiding the Monte Carlo sign problem.

3. The double-slit interference profile closely matches the empirical nanoscale data of Bach et al. (2013).

4. The transition from quantum superposition to the classical Born rule emerges directly from deterministic unitary entanglement into an orthogonal simulated environment.

A Numerical Details

The simulations were performed using vectorised arrays. The domain was a 2048×4096 grid. The boundary PML utilised a $\sin^2$ taper over 200 pixels. Evolution time was 2,200 steps. Execution time was approximately 90 seconds, demonstrating the extreme efficiency of direct unitary evolution compared to path sampling.

B Computational Implementation and Source Code

The complete, executable Python codebase along with the empirical dataset extracted from Bach et al. (2013) required to reproduce the numerical results has been made freely available in a public repository at: `https://github.com/dgedge/circlette-doubleslit.git`

To demonstrate the algorithmic simplicity of the discrete approach, the core kinematic engine is reproduced below. The entire physical universe of the simulation, including exact finite-difference propagation, dispersive mass, waveguide collimation, and unitary decoherence, is executed natively in fewer than 40 lines of local array operations:

```
# Core Lattice Evolution (2 Sub-lattices, 4 Spinor Components)
# psi.shape = (2, 4, HEIGHT, WIDTH)

c, s = np.cos(m), np.sin(m)

for t in range(STEPS):
    # 1. Spatial Shift (Propagation along routing channels)
    in0[:, :, 1:] = psi[:, 0, :, :-1]
    in0[:, :, 0] = 0
    in1[:, :, :-1] = psi[:, 1, :, 1:]
    in1[:, :, -1] = 0
    in2[:, 1:, :] = psi[:, 2, :-1, :]
    in2[:, 0, :] = 0
    in3[:, :-1, :] = psi[:, 3, 1:, :]
    in3[:, -1, :] = 0

    # 2. Vertex Summation
    sum_in = (in0 + in1 + in2 + in3) * 0.5
    v0, v1 = sum_in - in0, sum_in - in1
    v2, v3 = sum_in - in2, sum_in - in3

    # 3. Apply Chirality Coin U(m)
    psi[:, 0] = c * v0 - 1j * s * v1
    psi[:, 1] = c * v1 - 1j * s * v0
    psi[:, 2] = c * v2 - 1j * s * v3
    psi[:, 3] = c * v3 - 1j * s * v2

    # 4. Apply Physical Boundary Mask (Slits and Absorbing Sponge)
    psi[:, 0] *= mask
    psi[:, 1] *= mask
    psi[:, 2] *= mask
```

```
psi[:, 3] *= mask

# 5. Deterministic Unitary Decoherence (Measurement)
if measured:
    # True unitary SWAP between sub-lattices at Slit 1
    temp = psi[0, :, s1_slice, exit_x].copy()
    psi[0, :, s1_slice, exit_x] = psi[1, :, s1_slice, exit_x]
    psi[1, :, s1_slice, exit_x] = temp

# Accumulate photographic plate exposure
screen_exposure += np.sum(np.abs(psi[:, :, :, detector_x])**2, axis=(0, 1))
```

References

[1] A. Sommerfeld, Mathematische Theorie der Diffraction, Math. Ann. 47, 317 (1896).

[2] M. Gondran and A. Gondran, Numerical simulation of the double-slit interference with ultracold atoms, Am. J. Phys. 73, 507 (2005).

[3] R. Bach, D. Pope, S.-H. Liou, and H. Batelaan, Controlled double-slit electron diffraction, New Journal of Physics 15, 033018 (2013).

[4] H. D. Zeh, On the interpretation of measurement in quantum theory, Foundations of Physics 1, 69 (1970).

[5] W. H. Zurek, Quantum Darwinism, Nature Physics 5, 181-188 (2009).